Splicing factor SRSF1 is essential for homing of precursor spermatogonial stem cells in mice

Longjie Sun[1], Zheng Lv[1], Xuexue Chen[1], Rong Ye[4], Shuang Tian[1], Chaofan Wang[1], Xiaomei Xie[1], Lu Yan[1], Xiaohong Yao[1], Yujing Shao[1], Sheng Cui[3], Juan Chen[2, *], and Jiali Liu[1, *]

[1]State Key Laboratory of Animal Biotech Breeding, College of Biological Sciences, China Agricultural University, Beijing, 100193, China.

[2]Key Laboratory of Precision Nutrition and Food Quality, Department of Nutrition and Health, China Agricultural University, Beijing, 100190, China.

[3]College of Veterinary Medicine, Yangzhou University, Yangzhou, Jiangsu, 225009, China.

[4]Key Laboratory of RNA Biology, Institute of Biophysics, Chinese Academy of Sciences, Beijing, 100101, China.

*Correspondence: chenjuan.09@163.com (J.C.), liujiali@cau.edu.cn (J.L.)

Abstract

Spermatogonial stem cells (SSCs) are essential for continuous spermatogenesis and male fertility. The underlying mechanisms of alternative splicing (AS) in mouse SSCs are still largely unclear. We demonstrated that SRSF1 is essential for gene expression and splicing in mouse SSCs. Crosslinking immunoprecipitation and sequencing (CLIP-seq) data revealed that spermatogonia-related genes (e.g., *Plzf*, *Id4*, *Setdb1, Stra8*, *Tial1*/*Tiar*, *Bcas2*, *Ddx5*, *Srsf10*, *Uhrf1*, and *Bud31*) were bound by SRSF1 in the mouse testes. Specific deletion of *Srsf1* in mouse germ cells impairs homing of precursor SSCs leading to male infertility. Whole-mount staining data showed the absence of germ cells in the testes of adult cKO mice, which indicates Sertoli cell-only syndrome (SCOS) in cKO mice. The expression of spermatogonia-related genes (*Gfra1*, *Pou5f1*, *Plzf*, *Dnd1*, *Stra8*, and *Taf4b*) was significantly reduced in the testes of conditional knockout (cKO) mice. Moreover, multiomics analysis suggests that SRSF1 may affect survival of spermatogonia by directly binding and regulating *Tial1*/*Tiar* expression through AS. In addition, immunoprecipitation mass spectrometry (IP-MS) and co-immunoprecipitation (Co-IP) data showed that SRSF1 interacts with RNA splicing-related proteins (SART1, RBM15, and SRSF10). Collectively, our data reveal the critical role of SRSF1 in spermatogonia survival, which may provide a framework to elucidate the molecular mechanisms of the posttranscriptional network underlying homing of precursor SSCs.

Keywords

SRSF1, alternative splicing, infertility, Sertoli cell-only syndrome, precursor spermatogonial stem cells, homing of precursor SSCs

Introduction

SCOS, also known as del Castillo syndrome or germ cell aplasia, is one of the most common causes of severe non-obstructive azoospermia (NOA) (Wang et al., 2023). SCOS is the presence of only Sertoli cells in the testicular tubules of the testes, with no germ cells present (Juul et al., 2014; Wang *et al.*, 2023). It is well known that abnormal self-renewal and differentiation of SSCs leads to SCOS (Kanatsu-Shinohara and Shinohara, 2013; La and Hobbs, 2019b). In mice, gonocytes begin homing at 0 to 3 days postpartum (dpp) and then develop into SSCs at 4 to 6 dpp for continuous self-renewal and differentiation (Lee and Shinohara, 2011; McLean et al., 2003; Tan and Wilkinson, 2020). The mechanisms regulating homing of precursor SSCs are hence crucial for forming SSC pools and establishing niches (Oatley and Brinster, 2012). Spermatogonia migrate to form two distinct subtypes in mice. The first subtype develops into precursor SSCs that provide an SSC population for adult spermatogenesis, whereas the second subtype transitions directly to differentiated spermatogonia that contribute to the first round of spermatogenesis but do not self-renew (Kluin and de Rooij, 1981; Law et al., 2019). Therefore, homing of precursor SSCs to establish niches is essential for SSC self-renewal and differentiation.

Many transcription factors (e.g., FOXO1, PLZF, POU5F1, TAF4B, CHD4, BCL6B, BRACHYURY, ETV5, ID4, LHX1, POU3F1, DMRT1, NGN3, SOHLH1, SOHLH2, SOX3, and STAT3) promote SSC self-renewal and differentiation (Cafe et al., 2021; Song and Wilkinson, 2014). However, the molecular mechanisms of the posttranscriptional network underlying homing of precursor SSCs are not sufficiently clear. Previous studies have identified the key RNA-binding proteins DND1 and DDX5 in SSCs with a unique and dominant role in posttranscriptional regulation (Legrand et al., 2019; Yamaji et al., 2017). Surprisingly, recent studies have found that the RNA-binding proteins SRSF10, UHRF1, BUD31, and BCAS2 regulate AS in mouse spermatogonia (Liu et al., 2022; Liu et al., 2017; Qin et al., 2023; Zhou et al., 2022). It is well known that testes are rich in AS events (Mazin et al., 2021; Venables, 2002). Thus, understanding the mechanisms of AS in human reproduction can provide new insights into clinical diagnosis. However, the underlying mechanisms of how AS functions in homing of precursor SSCs are still largely unclear.

Serine/arginine-rich splicing factor 1 (SRSF1; previously SF2/ASF) is a widely studied and important splicing factor involved in cancer progression, heart development, and thymus development (Du et al., 2021; Katsuyama et al., 2019; Katsuyama and Moulton, 2021; Liu et al., 2021; Lv et al., 2021; Qi et al., 2021; Xu et al., 2005). Our previous work has shown that SRSF1 deficiency impairs primordial follicle

formation during meiotic prophase I and leads to primary ovarian insufficiency (POI) (Sun et al., 2023b). However, the underlying mechanisms by which SRSF1 regulates pre-mRNA splicing in mouse SSCs remain unknown. A mouse model with *Srsf1* conditional deletion can effectively address this uncertainty. This study showed that specific deletion of *Srsf1* in mouse germ cells leads to NOA by impairing homing of mouse precursor SSCs. We further verified that SRSF1 directly binds and regulates *Tial1*/*Tiar* expression via AS, which may be critical for homing of mouse precursor SSCs.

Results

SRSF1 may have a vital role in posttranscriptional regulation in the testes

To investigate the role of SRSF1 in spermatogenesis, the dynamic localization of SRSF1 in the testis was evaluated. Fascinatingly, the results of SRSF1 and γH2AX co-staining revealed that SRSF1 was expressed during spermatogenesis (Figure 1A and S1). RT–qPCR and Western blotting results showed that the expression of SRSF1 fluctuated during the developmental stages of the testes (Figure 1B and 1C). Concurrently, the results of SRSF1 and PLZF co-staining revealed that SRSF1 was highly expressed in the nuclei of spermatogonia (Figure 1D). To further explore the function of SRSF1 in regulating SSC self-renewal and differentiation, CLIP-seq was performed in adult mouse testes (Sun et al., 2023a). GO enrichment analyses of the SRSF1 peak-containing genes revealed that spermatogenesis-related genes were regulated by SRSF1 (Figure 2A and Table S1). In combination with previous studies, we found that spermatogonia-related genes (*Plzf*, *Id4*, *Setdb1, Stra8*, *Tial1*/*Tiar*, *Bcas2*, *Ddx5*, *Srsf10*, *Uhrf1*, and *Bud31*) were bound by SRSF1. To provide in-depth insight into the binding of spermatogonia-associated genes, the SRSF1-binding peaks of the gene transcripts were shown by using IGV (Figure 2B). The co-staining results showed localization and expression of the spermatogonia-related protein in mouse testes (Figure 2C). Together, these results suggested that SRSF1 may have a vital role in posttranscriptional regulation in the testes, particularly during spermatogonium development.

SRSF1 deficiency leads to SCOS

To define the specific involvement of SRSF1 in spermatogonia, we studied the physiological roles of SRSF1 in vivo using a mouse model. Considering that global SRSF1 knockout is lethal in mice (Xu *et al.*, 2005), we used a conditional allele of *Srsf1* (*Srsf1*^{Fl}) in which exons 2, 3, and 4 of *Srsf1* are flanked by two *loxP* sites (Figure 3A). By crossing *Srsf1*^{Fl} and *Vasa*-Cre mice, we obtained *Vasa*-Cre *Srsf1*$^{Fl/del}$ mice with *Srsf1* deletion in germ cells (Figure 3A and 3B). We verified the absence of the SRSF1 protein

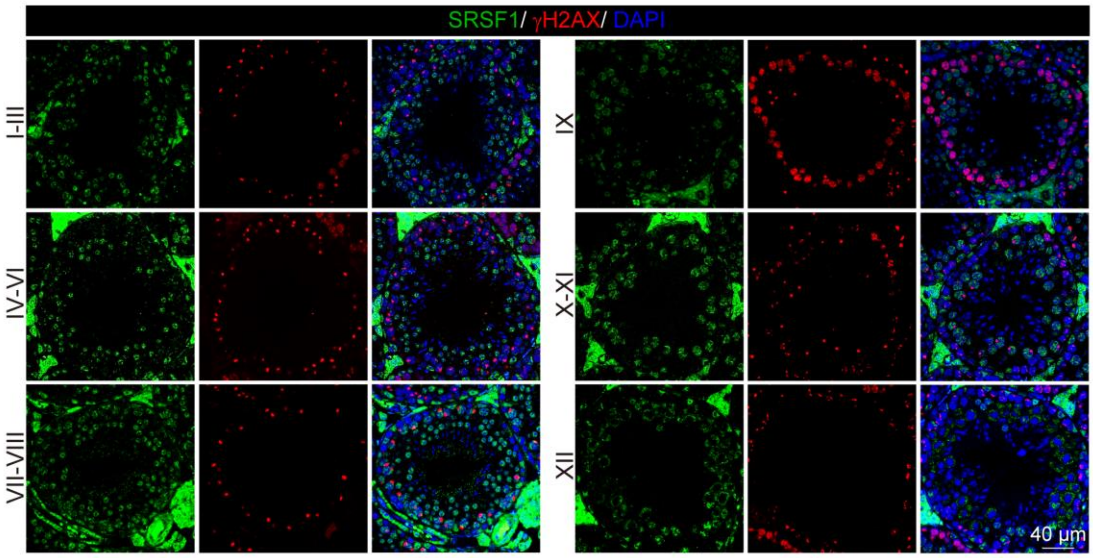

Figure S1. Dynamic localization of SRSF1 during spermatogenesis.

Co-immunostaining was performed using SRSF1 and γH2AX antibodies in adult mouse testes. DNA was stained with DAPI. Scale bar, 40 μm.

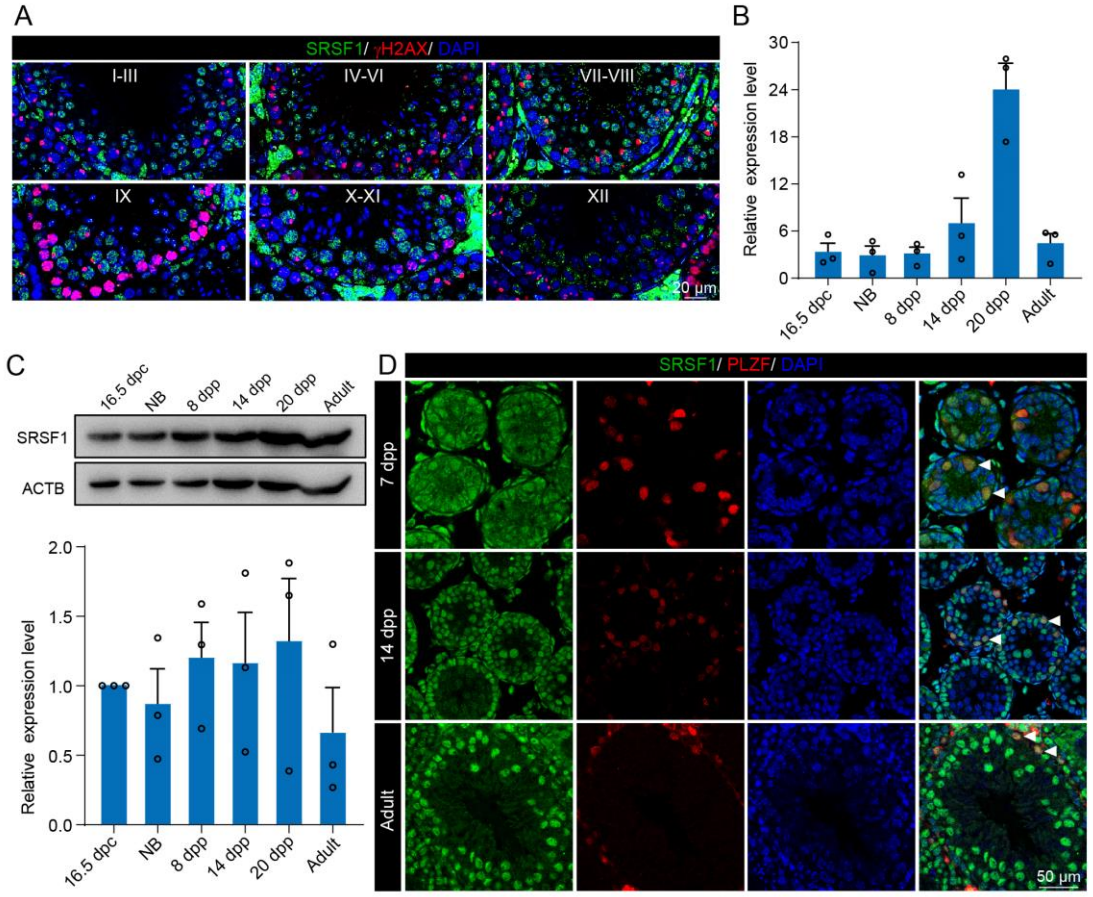

Figure 1 Dynamic localization of SRSF1 in male mouse germ cells.

(A) Dynamic localization of SRSF1 during spermatogenesis. Co-immunostaining was performed using SRSF1 and

γH2AX antibodies from adult mouse testes. DNA was stained with DAPI. Scale bar, 20 μm.

(B) Expression of *Srsf1* in testes at different stages of development. The RT–qPCR data were normalized to *Gapdh*. *n*=3.

(C) Western blotting of SRSF1 expression in testes at different stages of development. ACTB served as a loading control. The value in 16.5 dpc testes were set as 1.0, and the relative values of testes in other developmental periods are indicated. n=3.

(D) Localization and expression of SRSF1 in spermatogonia. Co-immunostaining was performed using PLZF and SRSF1 antibodies in 7 dpp, 14 dpp, and adult mouse testes. DNA was stained with DAPI. Arrowheads, spermatogonia. Scale bar, 50 μm

in germ cells by co-immunofluorescence analyses with SRSF1 and PLZF antibodies (Figure 3C). Subsequently, the breeding experiment indicated that cKO mice had a standard mating capacity but that the absence of *Srsf1* led to complete infertility in males (Figure 3D). Histological examination of cKO epididymides revealed that sperm could not be found in the cauda epididymis (Figure 3E). Considering the limitations of sectioning, the cauda epididymal sperm count further validated this conclusion (Figure 3F). It was clear that spermatogenesis in the testes was severely impaired. Therefore, we focused our attention on the testes. The adult cKO mice were normal in size (Figure 3G). However, the sizes of cKO mouse testes were significantly reduced (Figure 3H). Histological examination of cKO testis sections showed that no germ cells could be visualized, and only a large number of Sertoli cells were observed in the testes of cKO mice (Figure 3I). Together, these results demonstrated that SRSF1 is critical for spermatogenesis and that its absence leads to SCOS.

Loss of SRSF1 impairs spermatogonia survival.

To further confirm the absence of germ cells in the testes of cKO mice, PLZF and γH2AX co-staining was performed in adult mouse testes. These data suggested that SRSF1 deficiency impaired germ cell survival (Figure 4A). The results of VASA and TRA98 co-staining further confirmed this phenotype (Figure 4B). Considering the limitations of sectioning, we used whole-mount immunostaining to perform a comprehensive analysis and found that germ cells were indeed absent in the testes of adult cKO mice (Figure 4C). To dynamically analyse the loss of germ cells, we collected testes from 5 dpp, 7 dpp, and 14 dpp mice. Morphological results showed that the testes of 7 dpp and 14 dpp cKO mice were much smaller than those of Ctrl mice (Figure 5A). To determine the presence of germ cells in cKO testes, VASA staining was performed in 5 dpp, 7 dpp, and 14 dpp Ctrl and cKO testes. The results showed that

germ cells were still present in cKO mice but were significantly reduced in 7 dpp and 14 dpp cKO testes (Figure 5B). The germ cell count per tube showed a significant reduction in the number of 7 dpp and 14

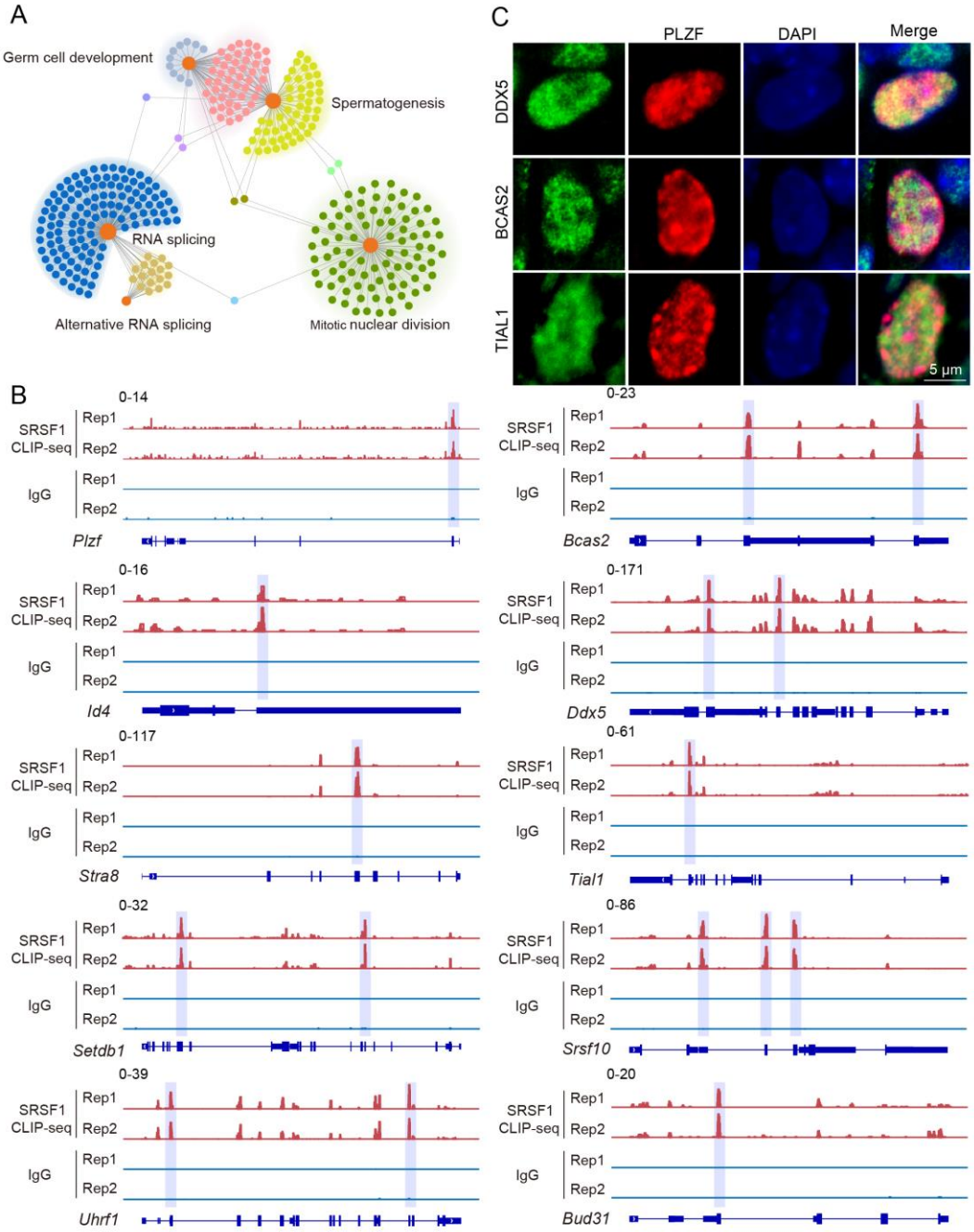

Figure 2 SRSF1-binding genes have an essential role in spermatogonia.

(A) Network showing GO enrichment analyses of SRSF1-binding genes.

(B) Representative genome browser views of spermatogonia-related gene transcripts bound by SRSF1. Higher peaks are marked by a lavender area.

(C) Localization and expression of the spermatogonia-related protein in mouse testes. Scale bar, 5 μm.

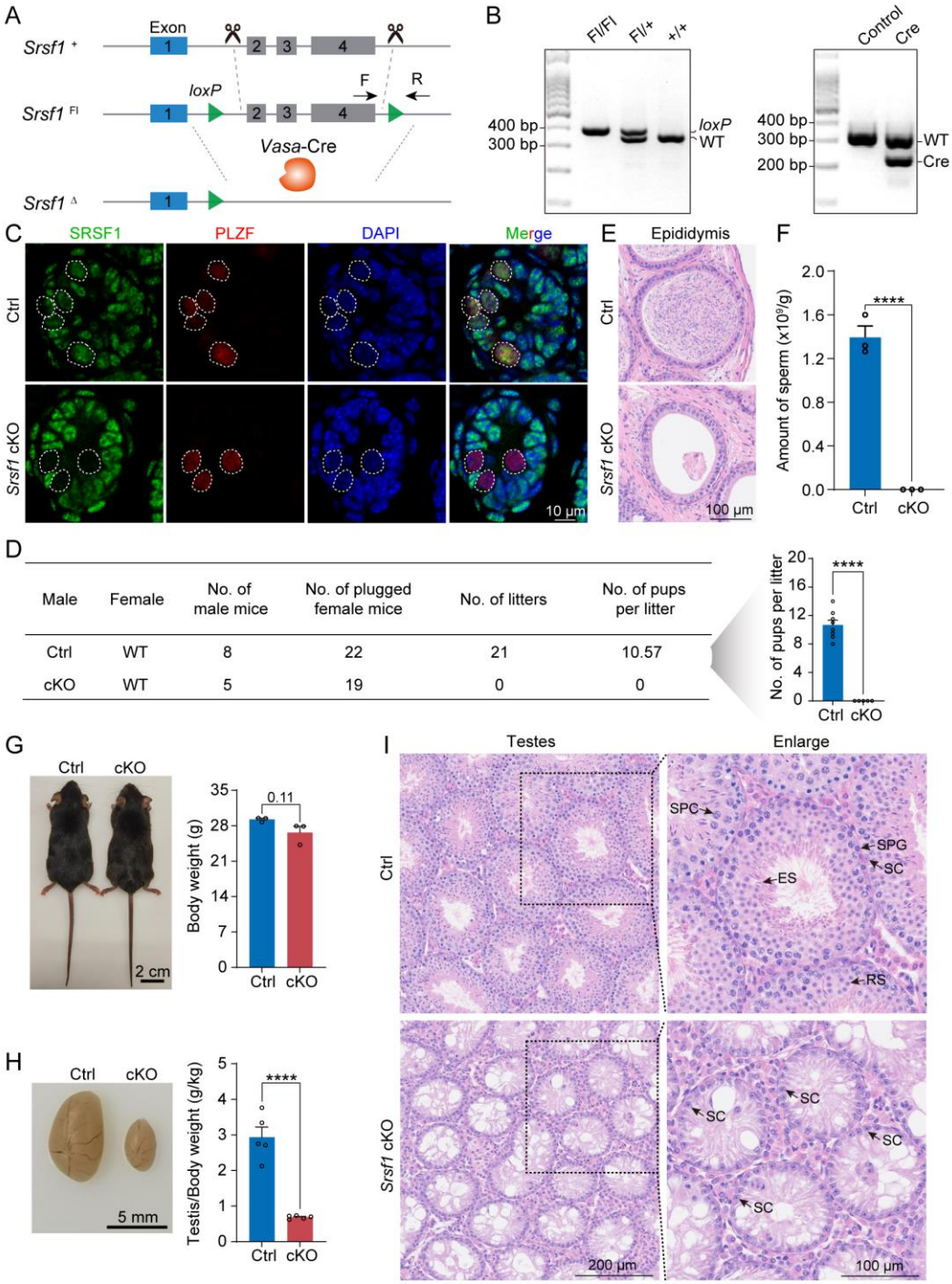

Figure 3 SRSF1 plays critical roles in spermatogenesis and male fertility.

(A) *Vasa*-Cre mice were crossed with *Srsf1*$^{Fl/Fl}$ mice to generate *Srsf1* cKO mice. Cre-mediated deletion removed exons 2, 3, and 4 of *Srsf1* and generated a null protein allele.

(B) Genotyping PCR was performed using *Vasa*-Cre and *Srsf1* primers.

(C) Co-immunostaining of SRSF1 and PLZF in 7 dpp Ctrl and cKO testes. DNA was stained with DAPI. Scale bar, 10 μm.

(D) Fertility test results showed a male infertility phenotype in the cKO mice (n= 5) compared to the Ctrl mice (n= 8).

The number of pups per litter was determined in the cKO (n= 5) and Ctrl (n= 8) mice.

(E) Haematoxylin-eosin-stained epididymis sections from adult Ctrl and cKO mice were obtained. Scale bar, 100 μm.

(F) Cauda epididymal sperm counting was performed. n=3.

(G) Normal body weight in cKO mice. The body sizes and weights of adult Ctrl and cKO mice are shown as the mean ± SEM. n= 3.

(H) Testis atrophy in adult cKO mice. Testis sizes and weights of adult Ctrl and cKO mice are shown as the mean ± SEM. n= 5.

(I) Haematoxylin-eosin-stained testis sections from adult Ctrl and cKO mice were obtained. Scale bar, left panel: 200 μm, right panel: 100 μm. SC, Sertoli cell; SPG, Spermatogonium; SPC, spermatocyte; RS, round spermatid; ES, elongated spermatid.

Unpaired Student's t test determined significance; exact P value $P \geq 0.05$, ****$P < 0.0001$. The points and error bars represent the mean ± SEM.

dpp cKO testes, especially 14 dpp cKO testes (Figure 5B). In addition, TUNEL results showed that apoptosis significantly increased in cKO testes (Figure 5C). These data suggested that the absence of SRSF1 causes apoptosis in a large number of spermatogonia that are unable to survive.

Loss of SRSF1 impairs homing of precursor SSCs

To further investigate the reason for the failure of spermatogonia to survive, we observed homing of precursor SSCs in the testes of mice at 5 dpp. Interestingly, the results of VASA and SOX9 co-staining showed that partial germ cells could not complete homing in 5 dpp cKO testes (Figure 6A and 6B). In mice, starting at 3 dpp, cytoplasmic FOXO1 in some gonocytes begins to enter the nucleus (Goertz *et al.*, 2011). These cells further develop into prospermatogonia, which are expected to develop into spermatogonial stem cells (Goertz *et al.*, 2011). Thus, immunohistochemical staining for FOXO1 was performed on 5 dpp mouse testis sections (Figure 6C). Further, germ cell statistics of FOXO1 expression in the nucleus showed a reduced number of prospermatogonia in cKO mice (Figure 6D). And germ cells in which FOXO1 is expressed in the nucleus similarly undergo abnormal homing (Figure 6E). Thus, all the above data indicated that SRSF1 has an essential role in the homing of precursor SSCs.

SRSF1 is essential for gene expression in spermatogonia

To investigate the molecular mechanisms of SRSF1 in spermatogonia, we isolated mRNA from 5 dpp cKO and Ctrl mouse testes and performed RNA-seq (Figure S2). RNA-seq and RT–qPCR results showed a significant reduction in the expression of *Srsf1* in 5 dpp cKO mouse testes (Figure 7A). Western

206

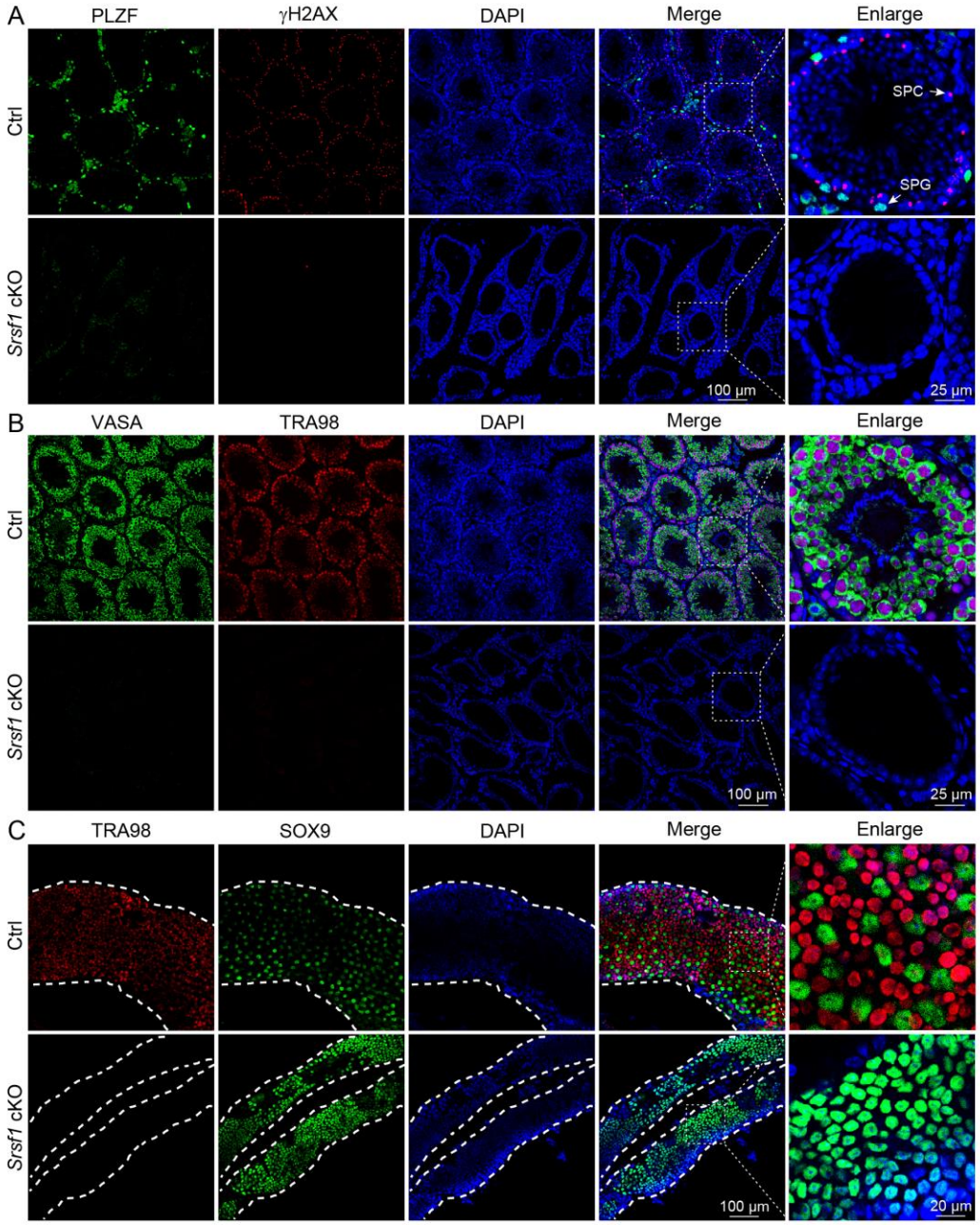

207

208 **Figure 4 Loss of germ cells in adult cKO mouse testes.**

209 (A) Co-immunostaining of PLZF and γH2AX in adult Ctrl and cKO testes. DNA was stained with DAPI. Scale bar,
210 right panel: 25 μm, other panels: 100 μm.

211 (B) Co-immunostaining of VASA and TRA98 in adult Ctrl and cKO testes. DNA was stained with DAPI. Scale bar,
212 right panel: 25 μm, other panels: 100 μm.

213 (C) Whole-mount co-immunostaining of TRA98 and SOX9 in adult Ctrl and cKO testes. DNA was stained with
214 DAPI. White dashed lines, boundary of the tubule. Scale bar, right panel: 20 μm, other panels: 100 μm.

215

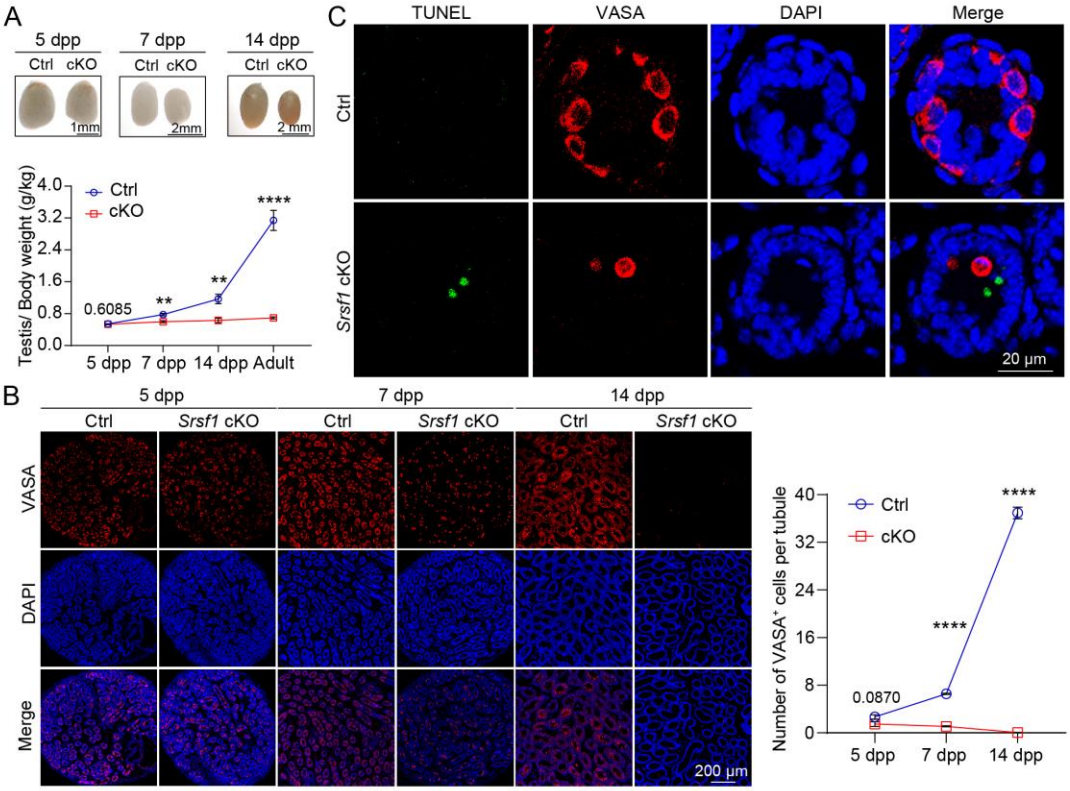

Figure 5 SRSF1 is required for spermatogonia survival.

(A) Testis sizes of 5 dpp, 7 dpp, and 14 dpp Ctrl and cKO mice are shown. The testis/body weight ratios (g/kg) of 5 dpp, 7 dpp, 14 dpp, and adult Ctrl and cKO mice are shown as the mean ± SEM. $n = 4$.

(B) Immunostaining of VASA in 5 dpp, 7 dpp, and 14 dpp Ctrl and cKO testes. DNA was stained with DAPI. Scale bar, 200 μm. Number of VASA-positive cells per tubule is the mean ± SEM. $n = 3$.

(C) TUNEL apoptosis assay was performed on sections from 7 dpp Ctrl and cKO testes. DNA was stained with DAPI. Scale bar, 20 μm.

Unpaired Student's *t* test determined significance; exact *P* value $P \geq 0.05$, $^{**}P < 0.01$, $^{****}P < 0.0001$. The points and error bars represent the mean ± SEM.

blotting results showed that SRSF1 expression was significantly reduced in the testes of cKO mice at 5 dpp (Figure 7B). Hence, for Ctrl and cKO samples, the confidence level of the RNA-seq data was high. The volcano map and cluster heatmap showed 715 downregulated and 258 upregulated genes identified by RNA-seq data in 5 dpp cKO mouse testes (Figure 7C, 7D and Table S2). These gene GO enrichment analyses indicated abnormal germ cell development and cell cycle arrest in 5 dpp cKO mouse testes (Figure 7E). Surprisingly, the heatmap showed that spermatogonia associated gene (*Gfra1*, *Pou5f1*, *Plzf*, *Nanos3*, *Dnd1*, *Stra8*, and *Taf4b*) expression was significantly reduced in the testes of cKO mice at 5 dpp

234 (Figure 7F). Simultaneously, visual analysis using IGV showed that the peak of SSC-related genes was
235 significantly decreased (Figure 7G). Next, we validated the abnormal expression of spermatogonia
236 associated genes (downregulated: *Gfra1*, *Pou5f1*, *Plzf*, *Dnd1*, *Stra8*, and *Taf4b*; stabilized: *Nanos3*) by
237 RT–qPCR (Figure 7H). Together, these data indicated that germ cell-specific deletion of *Srsf1* impairs
238 the expression of spermatogonia associated genes.

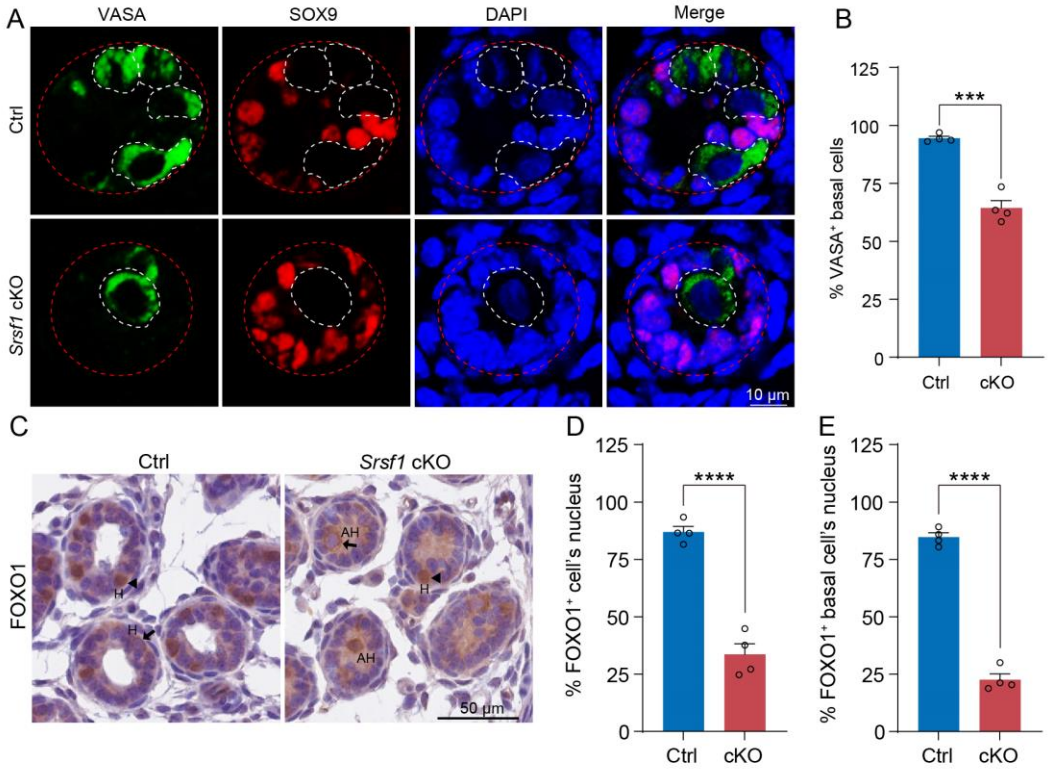

239

240 **Figure 6 SRSF1 is required for SSC homing of precursor SSCs.**

241 (A) Co-immunostaining of VASA and SOX9 in 5 dpp Ctrl and cKO testes. DNA was stained with DAPI. Scale bar,
242 10 μm. Red dashed circles, tubule. White dashed circles, germ cell.

243 (B) The percentage of VASA positive basal cells is shown as the mean ± SEM. $n = 4$.

244 (C) Immunohistochemistry staining of FOXO1 in 5 dpp Ctrl and cKO testes. The nuclei were stained with
245 haematoxylin. Scale bar, 10 μm. Arrowheads, FOXO1 in the nucleus. Arrows, FOXO1 in the cytoplasm. H, homing.
246 AH, abnormal homing.

247 (D) The percentage of FOXO1 positive cell's nucleus is shown as the mean ± SEM. $n = 4$.

248 (E) The percentage of FOXO1 positive basal cell's nucleus is shown as the mean ± SEM. $n = 4$.

249 Unpaired Student's *t* test determined significance; ***$P < 0.001$, ****$P < 0.0001$. The points and error bars represent
250 the mean ± SEM.

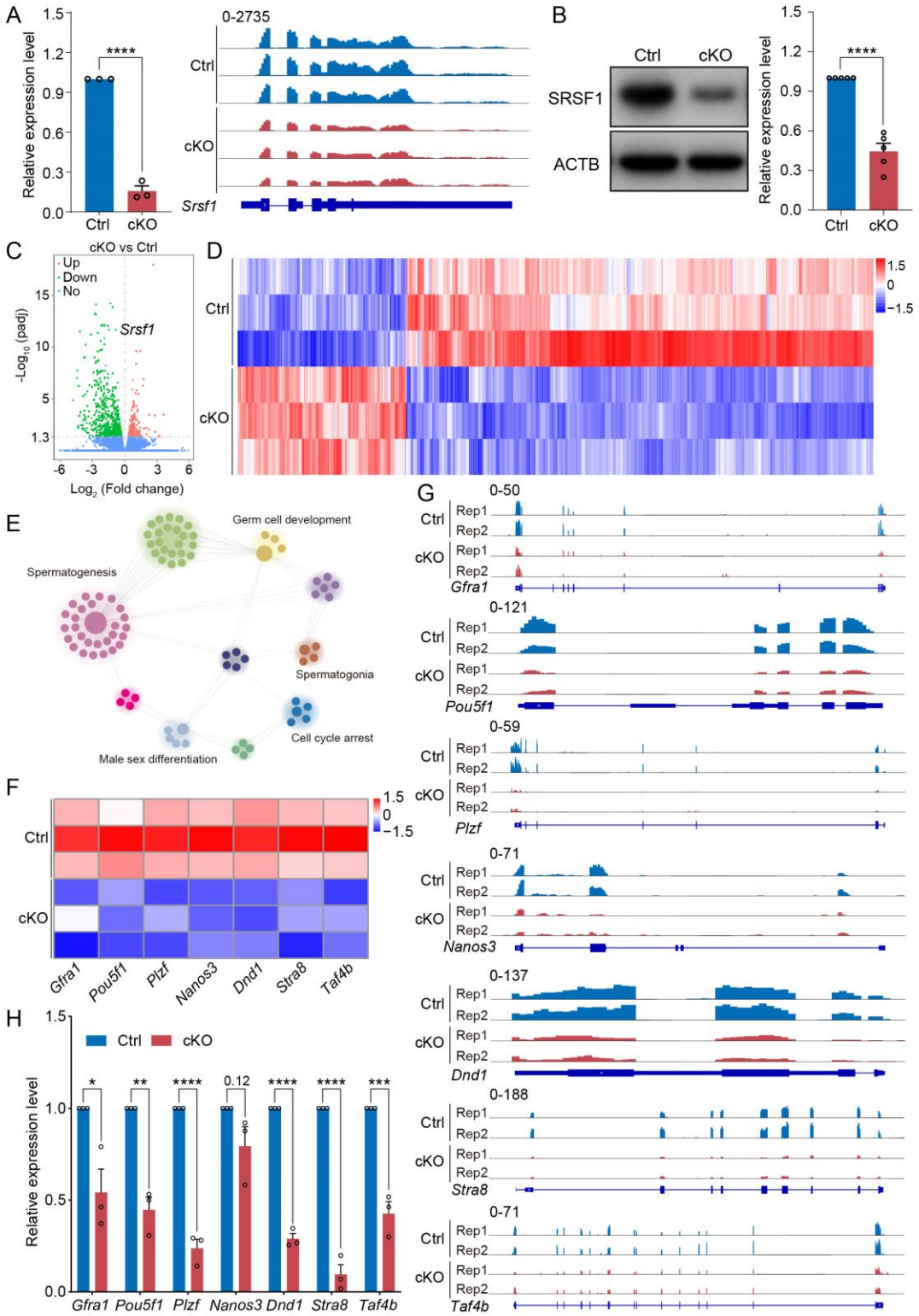

Figure 7 SRSF1 regulates the expression of spermatogonia-related genes.

(A) Expression of *Srsf1* in 5 dpp Ctrl and cKO mouse testes. The RT–qPCR data were normalized to *Gapdh*. *n*=5. The expression of *Srsf1* is shown as reading coverage in 5 dpp mouse testes.

(B) Western blotting of SRSF1 expression in 5 dpp mouse testes. ACTB served as a loading control. The value in

Ctrl testes was set as 1.0, and the relative values in cKO testes are indicated. *n*=5.

(C) Volcano map displaying the distribution of differentially expressed genes from RNA-seq data. The abscissa in the figure represents the gene fold change in 5 dpp cKO and Ctrl mouse testes. |log2FoldChange| ≥ 0. The ordinate indicates the significance of gene expression differences between 5 dpp cKO and Ctrl mouse testes. padj ≤ 0.05. Upregulated genes are shown as red dots, and downregulated genes are shown as green dots.

(D) Cluster heatmap of differentially expressed genes. The ordinate is the genotype, and the abscissa is the normalized FPKM (fragments per kilobase million) value of the differentially expressed gene. Red indicates a higher expression level, while blue indicates a lower expression level.

(E) Network showing GO enrichment analyses of differentially expressed genes.

(F) Heatmap of spermatogonia-related gene expression.

(G) The expression of spermatogonia-related genes is shown as read coverage.

(H) The expression of spermatogonia-related genes in 5 dpp cKO and Ctrl mouse testes. The RT–qPCR data were normalized to *Gapdh*. The value in the Ctrl group was set as 1.0, and the relative value in the cKO group is indicated. *n*=3. Unpaired Student's *t* test determined significance; exact *P* value $P \geq 0.05$, $^{*}P < 0.05$, $^{**}P < 0.01$, $^{***}P < 0.001$, $^{****}P < 0.0001$. The points and error bars represent the mean ± SEM.

SRSF1 directly binds and regulates the expression and AS of *Tial1*/*Tiar*

Multiomics analyses were carried out in a subsequent study to identify the molecular mechanisms by which SRSF1 regulates spermatogonia survival. Considering that the CLIP-seq data were obtained from adult mouse testis, the set of genes bound by CLIP-seq was restricted to those expressed only in the 5 dpp mouse testis RNA-seq data. we found that 3543 of the 4824 genes bound by SRSF1 were expressed in testes at 5 dpp. Venn diagram data revealed that nine out of 715 down-regulated genes were bound by SRSF1 and underwent abnormal AS (Figure 8A). And one out of 258 upregulated genes was bound by SRSF1 and underwent abnormal AS (Figure 8A). Interestingly, we found that 39 stabilized genes were bound by SRSF1 and underwent abnormal AS (Figure 8A). The AS genes were subsequently investigated in 5 dpp cKO mouse testes using transcriptomic analyses. RNA-seq analyses showed that 162 AS events were significantly affected (FDR<0.05) in cKO mouse testes (Figure 8B, 8C and Table S3). Most of the 133 affected AS events (162) were classified as skipped exons (SEs), with ten AS events categorized as retained introns (RIs), thirteen as mutually exclusive exons (MXEs), four as alternative 5' splice sites (A5SSs), and two as alternative 3' splice sites (A3SSs) (Figure 8C). Additionally, the overall analysis of aberrant AS events showed that SRSF1 effectively promotes the occurrence of SE and MXE events and inhibits the occurrence of RI events. (Figure 8C). Then, GO enrichment analyses of AS genes revealed

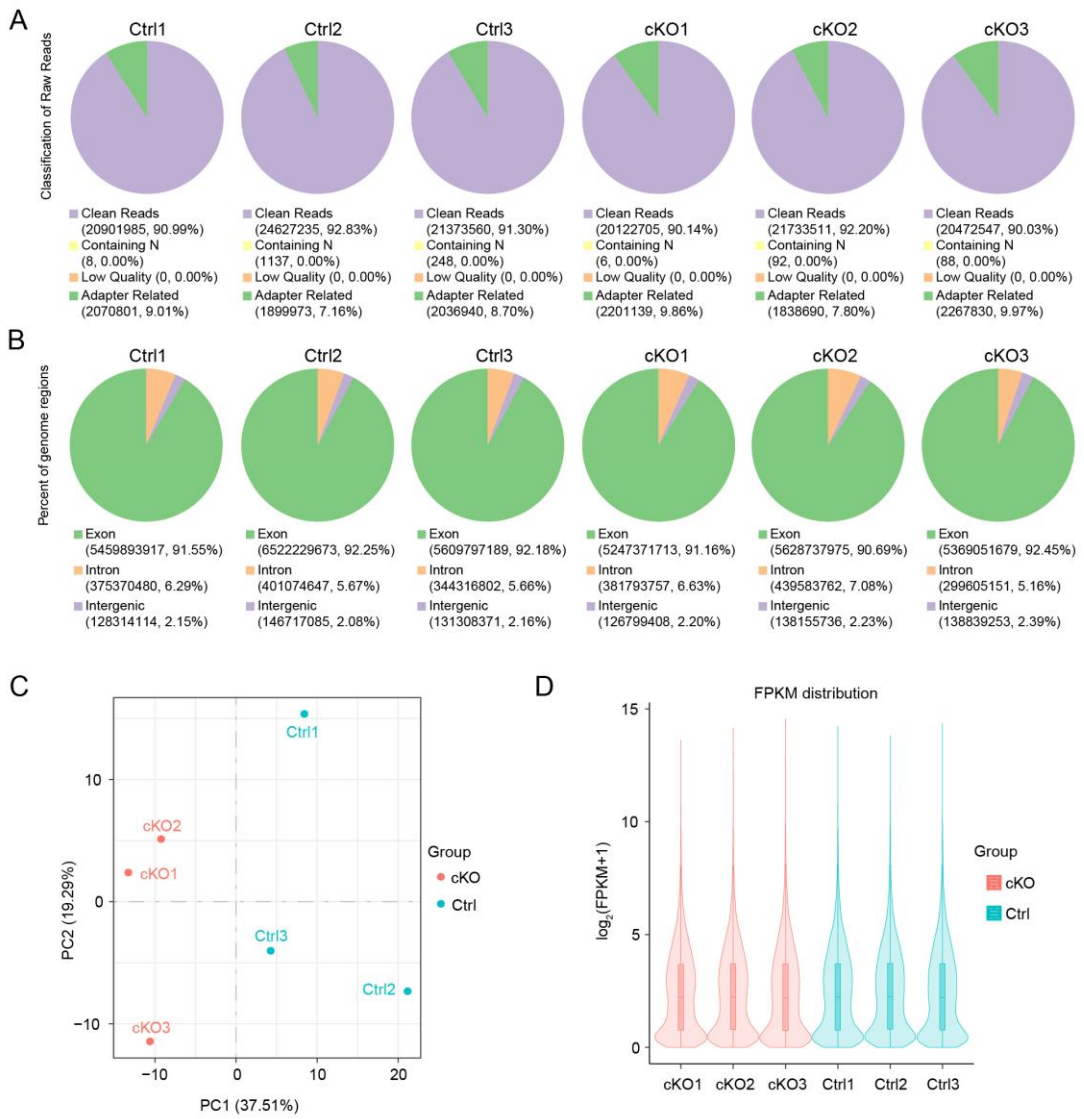

Figure S2. The libraries of RNA-seq are of good quality.

(A) Filtering of sequencing data per sample.

(B) Distribution of sequenced reads across genomic regions for all samples.

(C) Gene expression values (FPKM) of all samples were subjected to principal component analysis (PCA).

(D) The distribution of gene expression levels of different samples is demonstrated by violin plots as shown below. The horizontal coordinate of the graph is the name of the sample, and the vertical coordinate is $\log_2$ (FPKM+1).

that four genes concerning germ cell development were altered in AS forms (Figure 8D). It has been shown that *Tial1*/*Tiar* affects the survival of primordial germ cells (Beck et al., 1998). Moreover, *Tial1*/*Tiar* is one of 39 stabilizing genes that are bound by SRSF1 and undergo abnormal AS. Thus, multiomics analyses suggested that *Tial1*/*Tiar* were posttranscriptionally regulated by SRSF1. Next, we investigated the mechanism by which SRSF1 regulates the AS of *Tial1*/*Tiar*, RT–PCR results showed

that the pre-mRNA of *Tial1*/*Tiar* in 5 dpp cKO mouse testes exhibited abnormal AS (Figure 8E). We then visualized the different types of AS based on RNA-seq data by using IGV (Figure 8F). The results of RIP–qPCR showed that SRSF1 could bind to the pre-mRNA of *Tial1*/*Tiar* (Figure 8G). Interestingly, RNA-seq analyses showed that the FPKM of *Tial1*/*Tiar* was stabilized in 5 dpp cKO mouse testes (Figure 8H). RT–qPCR results showed that *Tial1*/*Tiar* transcript levels were not inhibited (Figure 8I). However, Western blotting showed that expression levels of TIAL1/TIAR isoform X2 were significantly suppressed (Figure 8J). In summary, the data indicate that SRSF1 is required for TIAL1/TIAR expression and splicing in spermatogonia survival.

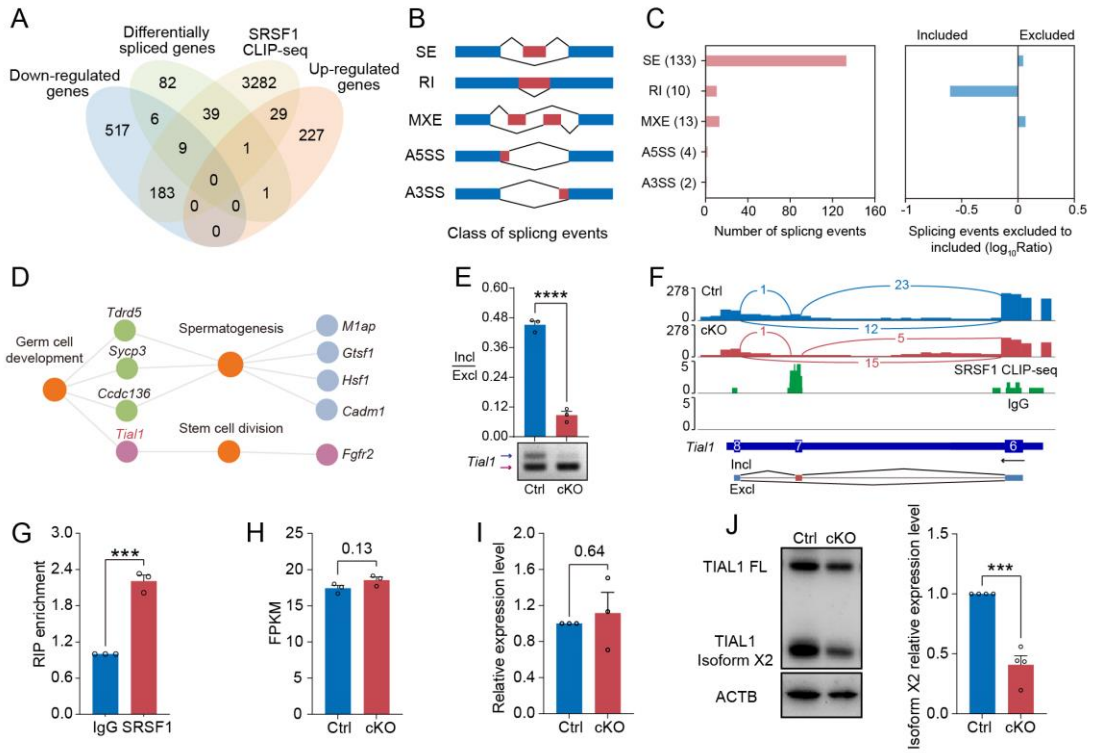

Figure 8 SRSF1 directly binds and regulates the expression and AS of *Tial1*/*Tiar*.

(A) Venn diagram showing the correlation among down-regulated, upregulated, alternatively spliced, and SRSF1-binding genes.

(B) Schematic diagram showing the classes of splicing events.

(C) Splicing events were analysed by number, exclusion, and inclusion.

(D) Network showing GO enrichment analyses of AS genes.

(E) The ectopic splicing of *Tial1/Tiar* in 5 dpp cKO and Ctrl mouse testes was analysed by RT–PCR. *n*=3. The ratio of inclusion (Incl) to exclusion (Excl) is shown accordingly.

(F) Analyses of *Tial1/Tiar* expression and exon–exon junctions were performed.

(G) SRSF1 directly binds the pre-mRNA of *Tial1*/*Tiar* by RIP–qPCR in 5 dpp mouse testes. *n*=3.

(H) The FPKM of *Tial1*/*Tiar* in 5 dpp cKO and Ctrl mouse testes.

(I) The expression of *Tial1*/*Tiar* in 5 dpp cKO and Ctrl mouse testes. The RT–qPCR data were normalized to *Gapdh*. The value in the Ctrl group was set as 1.0, and the relative value in the cKO group is indicated. n=3.

(J) Western blotting of TIAL1/TIAR expression in 5 dpp mouse testes. ACTB served as a loading control. The isoform X2/FL value of TIAL1/TIAR in the Ctrl group was set as 1.0, and the relative value in the cKO group is indicated. n=3. FL, Full length.

Unpaired Student's t test determined significance; exact P value $P \geq 0.05$, ***$P < 0.001$, ****$P < 0.0001$. The points and error bars represent the mean ± SEM.

SRSF1 recruits AS-related proteins to modulate AS in testes

To identify the interacting proteins for which SRSF1 exerts its AS role, we performed MS analyses of IP samples from 5 dpp mouse testis extracts. The silver-stained gel of SRSF1 and normal IgG showed several SRSF1-interacting proteins from 5 dpp mouse testis extracts (Figure 9A). The IP results indicated that SRSF1 was able to effectively IP the testis extracts of 5 dpp mice (Figure 9B). IP-MS data demonstrated the efficient enrichment of SRSF1 (Figure 9C and Table S4). These data showed that the two samples were highly reproducible, especially for SRSF1 (Figure 9D). Then, GO enrichment analyses of the IP proteins revealed that AS-related proteins could interact with SRSF1 (Figure 8E). A circular heatmap showed that SRSF1 could interact with AS-related proteins (e.g., SRSF10, SART1, RBM15, SRRM2, SF3B6, and SF3A2) (Figure 9F). The Co-IP results indicated that FLAG-SRSF1 interacted with HA-SART1, HA-RBM15 and HA-SRSF10 in 293T cells (Figure 9G). In addition, the fluorescence results showed complete co-localization of mCherry-SRSF1 with eGFP-SART1, eGFP-RBM15 and eGFP-SRSF10 in 293T cells (Figure 9H). Co-IP suggested that the RRM1 domain of SRSF1 interacted with both HA-TRA2B and HA-U2AF2 in 293T cells (Figure 9I). Determining the complex structures of these interactions is valuable, in which molecular docking has played an important role (Yan et al., 2017). HDOCK is a novel web server of our hybrid docking algorithm of template-based modelling and free docking (Yan *et al.*, 2017). The HDOCK analysis results depicted the RRM1 domain of SRSF1 with SRSF10, SART1, and RBM15 docking based on a hybrid strategy (Figure 9J). Together, the above data show that SRSF1 may interact with SRSF10, SART1, and RBM15 to regulate AS in 5 dpp mouse testes.

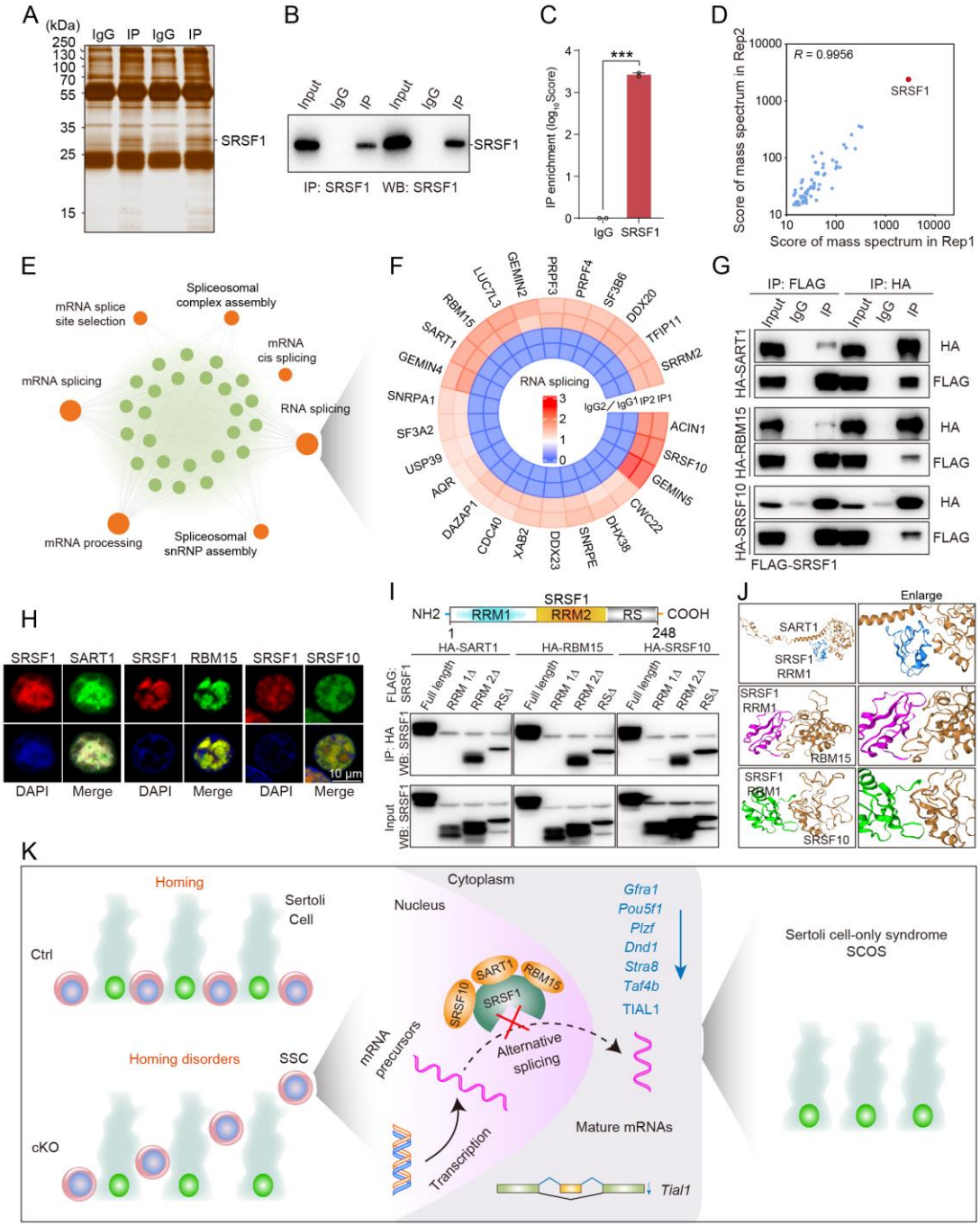

348

349 **Figure 9 SRSF1 recruits AS-related proteins to modulate AS in testes.**

350 (A) Silver-stained gel of SRSF1 and control immunoprecipitates from 5 dpp mouse testis extracts.

351 (B) IP experiment was performed in 5 dpp mouse testis extracts.

352 (C) IP of SRSF1 from IP-MS data.

353 (D) *Pearson's* correlation analysis showed the coefficient between the two samples for IP-MS data.

354 (E) Network showing GO enrichment analyses of SRSF1-binding proteins.

355 (F) Circular heatmap of AS-related proteins.

356 (G) Co-IP experiment for detecting the SRSF1 association between SART1, RBM15, and SRSF10 in 293T cells.

(H) SRSF1-mCherry cotransfected with SART1-eGFP, RBM15-eGFP, and SRSF10-eGFP 293T cells is shown. DNA was stained with DAPI. Scale bar, 10 μm.

(I) Co-IP experiment for detecting the SRSF1 truncated protein association between SART1, RBM15, and SRSF10 in 293T cells.

(J) A schematic diagram of protein interactions is shown.

(K) Schematic illustration of the molecular mechanisms by which SRSF1 regulates homing of mouse precursor SSCs.

Discussion

Failure of spermatogonia survival led to SCOS

Disturbed spermatogenesis can cause SCOS and ultimately male sterility (Jiao et al., 2021). In recent years, it has been reported that many spermatogonia-related gene deletions have disrupted SSC self-renewal and differentiation in patient and mouse models (La and Hobbs, 2019a; Tan and Wilkinson, 2020; Wang et al., 2021). SCOS was observed in *Ddx5*, *Tial1*/*Tiar*, *Uhrf1*, *Pramef12*, *Dot1l*, and *Rad51* deletion mouse models (Beck *et al.*, 1998; Legrand *et al.*, 2019; Lin et al., 2022; Qin et al., 2022; Wang et al., 2019; Zhou *et al.*, 2022). Mouse models are still of great significance and reference for human SCOS studies, and they will provide a better understanding of how SCOS occurs and develops over time. Interestingly, our mouse model had SCOS (Figure 3D-I and Figure 4). The absence of germ cells represents classical SCOS in adult mouse testes (Figure 4) (Wang *et al.*, 2023). In addition, we found abnormal expression of spermatogonia-related genes (*Gfra1*, *Pou5f1*, *Plzf*, *Dnd1*, *Stra8*, and *Taf4b*) in cKO mouse testes (Figure 7F-H). These differentially expressed genes regulate SSC self-renewal and differentiation in mouse testes (Kanatsu-Shinohara and Shinohara, 2013; La and Hobbs, 2019a; Tan and Wilkinson, 2020). Thus, this provided an opportunity for us to better study the underlying molecular mechanisms. These data indicate that SRSF1 deficiency impairs spermatogonia survival, leading to SCOS in male mice.

The formation of SSC pools and the establishment of niches are essential for spermatogenesis

The earliest event in the development of the SSC population is the migration of prospermatogonia from the centre of seminiferous cords where they have resided since sex determination of the embryonic gonad to the basement membrane (Oatley and Brinster, 2012). In mice, this process is also known as homing of precursor SSCs, which occurs in the first 3 dpp and then develops into SSCs at 4 to 6 dpp for continuous self-renewal and differentiation (Lee and Shinohara, 2011; McLean *et al.*, 2003; Oatley and Brinster, 2012; Tan and Wilkinson, 2020). Therefore, homing analysis of precursor SSCs was performed in 5 dpp

388 cKO mouse testes. Interestingly, the VASA and SOX9 co-staining results demonstrated that partial germ
389 cells could not complete homing in 5 dpp cKO testes (Figure 6A and 6B). Further, immunohistochemical
390 staining for FOXO1 and statistical results indicated that germ cells in which FOXO1 is expressed in the
391 nucleus similarly undergo abnormal homing (Figure 6C-E). Germ cells that do not migrate to the
392 basement membrane are unable to form SSC pools and establish niches (McLean *et al.*, 2003). These
393 SSCs that lose their ecological niche will cease to exist. In our data, TUNEL results showed that apoptosis
394 significantly increased in 7 dpp cKO mouse testes. At once, the germ cell count per tube showed a
395 significant reduction in 7 dpp and 14 dpp cKO testes, especially 14 dpp cKO testes (Figure 5B). In
396 conclusion, SRSF1 is crucial for the formation of SSC pools and the establishment of niches through
397 homing of precursor SSCs.

398 **Abnormal AS of *Tial1*/*Tiar* impaired the survival of spermatogonia**

399 AS is commonly found in mammals, especially in the brain and testes (Mazin *et al.*, 2021; Merkin et al.,
400 2012; Wang et al., 2008). AS plays essential roles in the posttranscriptional regulation of gene expression
401 during many developmental processes, such as SSC self-renewal and differentiation (Chen et al., 2018;
402 Song et al., 2020). Recently, BUD31-mediated AS of *Cdk2* was shown to be required for SSC self-
403 renewal and differentiation (Qin *et al.*, 2023). *Srsf10* depletion disturbed the AS of genes, including *Nasp*,
404 *Bclaf1*, *Rif1*, *Dazl*, *Kit*, *Ret*, and *Sycp1* (Liu *et al.*, 2022). UHRF1 interacts with snRNAs and regulates
405 AS of *Tle3* in mouse SSCs (Zhou *et al.*, 2022). Mettl3-mediated m6A regulates AS of *Sohlh1* and *Dazl*
406 (Xu et al., 2017). We found that SRSF1 acts as an alternative RNA splicing regulator and directly interacts
407 with *Tial1*/*Tiar* transcripts to regulate splicing events in spermatogonia (Figure 8E-G). Additionally,
408 expression levels of TIAL1/TIAR isoform X2 were significantly suppressed (Figure 8J). Interestingly,
409 *Tial1*/*Tiar* transcript levels were not inhibited (Figure 8H and 8I). These results suggested that SRSF1
410 explicitly regulates the expression of *Tial1*/*Tiar* via AS. Studies have reported that TIAL1/TIAR is
411 essential for primordial germ cell development in mouse testes (Beck *et al.*, 1998). *Tial1/Tiar* deletion
412 impairs spermatogonia survival leading to SCOS, consistent with our phenotype (Figure 3E-I and 4A-C)
413 (Beck *et al.*, 1998). Taken together, SRSF1 may affect spermatogonia survival by directly binding and
414 regulating *Tial1*/*Tiar* expression through AS.

415 We found that SRSF1 could interact with AS-related proteins (e.g., SRSF10, SART1, RBM15, SRRM2,
416 SF3B6, and SF3A2) (Figure 9F). A recent study reported that SRSF10 deficiency impaired
417 spermatogonia differentiation but did not affect homing of precursor SSCs (Liu *et al.*, 2022). However,

our data showed that SRSF1 is essential for homing of mouse precursor SSCs. Therefore, this suggests that SRSF1 has a specific function in the homing of precursor SSCs that are not bound by SRSF10.

SRSF1-mediated posttranscriptional regulation during homing of precursor SSCs provides new insights into the treatment of human reproductive diseases

Aberrant homing of precursor SSCs often lead to gametogenic failure or produce aneuploid gametes, resulting in subfertility or infertility, miscarriage, or congenital disabilities (Jiao *et al.*, 2021; Kanatsu-Shinohara and Shinohara, 2013; La and Hobbs, 2019a; Song and Wilkinson, 2014). Loss-of-function mutations in humans and corresponding knockout/mutated mice have been extensively researched (Jiao *et al.*, 2021). However, AS-related posttranscriptional regulation during meiosis has not been well studied. In recent years, there have been reports that the RNA-binding proteins SRSF10, UHRF1, BUD31, and BCAS2 regulate AS in mouse SSCs (Liu *et al.*, 2022; Liu *et al.*, 2017; Qin *et al.*, 2023; Zhou *et al.*, 2022). This study used a multiomics approach to perform in-depth analyses of SRSF1-mediated posttranscriptional regulatory mechanisms to enrich the field. It also provides new ideas and insights for clinical diagnosis and treatment.

In summary, this study demonstrates that SRSF1 plays a critical role in posttranscriptional regulation to implement homing of precursor SSCs (Figure 9K). Thus, the posttranscriptional regulation of SRSF1-mediated splicing is resolved during the formation of SSC pools and the establishment of niches.

Materials and Methods

Mouse strains

C57BL/6N and ICR mice were purchased from Beijing Vital River Laboratory Animal Technology Co., Ltd. *Srsf1*$^{Fl/Fl}$ mice were generated in the laboratory of Prof. Xiangdong Fu (University of California, San Diego, USA) and were kindly provided by Prof. Yuanchao Xue (Institute of Biophysics, Chinese Academy of Sciences, Beijing, China) (Xu *et al.*, 2005). *Vasa*-Cre mice were obtained from The Jackson Laboratory (Gallardo et al., 2007).To generate *Srsf1* cKO mice, *Vasa*-Cre mice were crossed with *Srsf1*$^{Fl/Fl}$ mice. The primers used for PCR to genotype *Srsf1*$^{Fl/Fl}$ and *Vasa*-Cre mice are shown in Table S5. All mice were bred and housed under specific pathogen-free conditions with a controlled temperature (22 ± 1°C) and exposed to a constant 12-hour light-dark cycle in the animal facilities of China Agricultural University. All experiments were conducted according to the guidelines and with the

447 approval of the Institutional Animal Care and Use Committee of China Agricultural University (No.
448 AW80401202-3-3).

449 **Fertility test**

450 For 15 days, two 8-week-old ICR female mice were caged with one 8-week-old male control (Ctrl) or
451 cKO mouse. The mice were kept individually after the appearance of the vaginal plug, and the dates were
452 recorded. Male mice continue to be caged after two days. The number of pups from each female was
453 recorded each day, and the date of parturition was recorded.

454 **Immunostaining and histological analyses**

455 Mouse testes were fixed with 4% paraformaldehyde (PFA, P6148-500G, Sigma–Aldrich) in PBS (pH
456 7.4) at 4°C overnight, dehydrated in graded ethanol solutions, vitrified with xylene, and embedded in
457 paraffin. Testis sections were cut at a 5-μm thickness for immunostaining and histologic analyses. For
458 histological analyses, sections were dewaxed in xylene, rehydrated in a graded ethanol solution, and
459 stained with haematoxylin-eosin. After sealing the slides with neutral resin, a Ventana DP200 system was
460 used for imaging. For immunofluorescence analyses, antigen retrieval was performed by microwaving
461 the sections with sodium citrate buffer (pH 6.0). After blocking with 10% normal goat serum at room
462 temperature for 1 hour, the sections were incubated with primary antibodies (Table S6) in 5% normal
463 goat serum overnight at 4°C. After washing with PBS, the sections were incubated with secondary
464 antibodies (Table S6) at room temperature in the dark for 1 hour. The slides were mounted in an antifade
465 mounting medium with DAPI (P0131, Beyotime). Photographs were taken with a Nikon A1 laser
466 scanning confocal microscope and a Zeiss OPTOME fluorescence microscope. For
467 immunohistochemistry analyses, antigen retrieval was performed by microwaving the sections with
468 sodium citrate buffer (pH 6.0). 5 dpp testis sections were prepared as described in the instructions for
469 Immunohistochemistry Kit (PV-9001, ZSGB-BIO). After sealing the slides with neutral resin, a Ventana
470 DP200 system was used for imaging.

471 **Whole-mount immunostaining**

472 The testes were collected and dispersed with 5ml syringes. Blown-out tubules were fixed in PFA at 4°C
473 for 4 hours. The tubules were washed three times with PBS (pH 7.4) for 5 min each and stored at 4°C.
474 The tubules were permeated with 0.3% Triton X-100 for 1 h at 4°C. Then, whole-mount staining followed
475 the immunostaining protocol.

476 **TUNEL apoptosis analyses**

477 7 dpp testis sections were prepared as described in the instructions for the TUNEL Apoptosis Assay Kit
478 (C1088, Beyotime). Photographs were taken with a Nikon A1 laser scanning confocal microscope and a
479 Zeiss OPTOME fluorescence microscope.

480 **RT–PCR and RT–qPCR**

481 Total RNA was extracted by using RNAiso Plus (9109, Takara), and the concentration was measured
482 with a Nano-300 ultramicro spectrophotometer (Allsheng). cDNA was obtained according to the
483 instructions of a TIANScript II RT kit (KR107, TIANGEN). The expression of transcripts of the target
484 gene was measured by using a LightCycle® 96 instrument (Roche) with Hieff UNICON SYBR green
485 master mix (11198ES08, Yeasen). AS analyses were performed on a RePure-A PCR instrument (BIO-
486 GENER). Primers were synthesized by Sangon Biotech (Table S5). The expression level of *Gapdh* or
487 *Actb* was used as the control, and this value was set as 1. Other samples' relative transcript expression
488 levels were obtained by comparing them with the control results.

489 **RNA-seq**

490 Total RNA was extracted from mouse testes according to the above protocol at 5 dpp. Briefly, mRNA
491 was purified from total RNA using poly-T oligo-attached magnetic beads. After fragmentation, we
492 established a transcriptome sequencing library and assessed library quality on an Agilent Bioanalyzer
493 2100 system. The clustering of the index-coded samples was performed on a cBot Cluster Generation
494 System using a TruSeq PE Cluster kit v3-cBot-HS (Illumina) according to the manufacturer's instructions.
495 After cluster generation, the library preparations were sequenced on the Illumina NovaSeq platform, and
496 150 bp paired-end reads were generated. After quality control, all downstream analyses were performed
497 on clean, high-quality data. The reference genome index was built, and paired-end clean reads were
498 aligned to the reference genome using HISAT2 software (version 2.0.5). FeatureCounts (version 1.5.0)
499 counted the reads mapped to each gene. Then, the fragments per kilobase million (FPKM) value of each
500 gene was calculated based on the length of the gene and the read count mapped to this gene. Differential
501 expression analyses of cKO/Ctrl mouse testes (three biological replicates per condition) were performed
502 using the DESeq2 R package (version 1.20.0). Genes with a padj ≤ 0.05 identified by DESeq2 were
503 considered differentially expressed.

504 **AS analyses**

505 rMATS software (version 3.2.5) was used to analyse the AS events in cKO mouse germ cells based on
506 RNA-seq data. Five types of AS events (SE, RI, MXE, A5SS, and A3SS) were revealed by rMATS

507 software. Our threshold for screening differentially significant AS events was a false discovery rate (FDR)
508 of less than 0.05. Splicing events with an FDR less than 0.05 and an inclusion-level difference with a
509 significance of at least 5% (0.05) were considered statistically significant. Integrative Genomics Viewer
510 (IGV, 2.16.0) software was used to visualize and confirm AS events based on RNA-seq data.

511 **Gene Ontology (GO) enrichment analyses**

512 The GO enrichment analyses of differentially expressed genes and AS genes were implemented with the
513 clusterProfiler R package (version 3.4.4), in which gene length bias was corrected. All expressed genes
514 (TPM sum of all samples >=1) are listed background. GRCm38/mm10 was used as a mouse reference
515 genome, and the Benjamini–Hochberg multiple methods was applied to adjust for multiple testing. GO
516 enrichment analyses with corrected *P* values of less than 0.05 were significantly enriched for
517 differentially expressed genes and AS genes.

518 **Western blotting**

519 Total protein was extracted with cell lysis buffer (P0013, Beyotime) containing PMSF (1:100, ST506,
520 Beyotime) and a protease inhibitor cocktail (1:100, P1005, Beyotime). A BCA protein assay kit
521 (CW0014S, CWBiotech) measured the protein concentration. The protein lysates were
522 electrophoretically separated on sodium dodecyl sulfate-polyacrylamide gels and electrically transferred
523 to polyvinylidene fluoride membranes (IPVH00010, Millipore). The membranes were blocked in 5%
524 skimmed milk for 1 hour and incubated with the primary antibodies (Table S6) for one night at 4°C. Then,
525 the membranes were incubated with secondary antibodies (Table S6) at room temperature for 1 hour. The
526 proteins were visualized using a Tanon 5200 chemiluminescence imaging system following incubation
527 with BeyoECL Plus (P0018S, Beyotime).

528 **IP, IP-MS, Co-IP**

529 Total protein was extracted with cell lysis buffer (P0013, Beyotime) containing PMSF (1:100, ST506,
530 Beyotime) and a protease inhibitor cocktail (1:100, P1005, Beyotime). After incubation on ice for 20 min,
531 the lysate was added to 20 μl of protein A agarose (P2051-2 ml, Beyotime) for pre-clearing at 4°C for 1
532 hour. Two micrograms of an SRSF1 antibody (sc-33652, Santa Cruz Biotechnology) and a normal mouse
533 IgG (sc-3879, Santa Cruz Biotechnology) were added to the lysate the mixture was incubated overnight
534 incubation at 4°C. The next day, 60 μl of protein A agarose was added to the lysate, which was then
535 incubated at 4°C for 4 hours. The agarose complexes containing antibodies and target proteins were
536 washed 3 times for 5 min at 4°C. IP and Co-IP were performed according to the above Western blotting

protocol. The complex was sent to the protein mass spectrometry laboratory for IP-MS analyses using a Thermo Q-Exactive high-resolution mass spectrometer (Thermo Scientific, Waltham). Raw data from the mass spectrometer were preprocessed with Mascot Distiller 2.4 for peak picking. The resulting peak lists were searched against the uniport mouse database using Mascot 2.5 search engine.

RNA immunoprecipitation (RIP) and RIP–qPCR

As described previously (Gagliardi and Matarazzo, 2016), RIP was performed using 5 dpp mouse testes. The testes were lysed in cell lysis buffer (P0013, Beyotime) containing PMSF (1:100, ST506, Beyotime), a proteinase inhibitor cocktail (1:100, P1005, Beyotime), DTT (1:50, ST041-2 ml, Beyotime), and an RNase inhibitor (1:20, R0102-10 kU, Beyotime). After incubation on ice for 20 min, the lysate was added to 20 μl of protein A agarose (P2051-2 ml, Beyotime) for pre-clearing at 4°C for 1 hour. Two micrograms of an SRSF1 antibody (sc-33652, Santa Cruz Biotechnology) and a normal mouse IgG (sc-3879, Santa Cruz Biotechnology) were added to the lysate, which was then incubated overnight at 4°C. The next day, 60 μl of protein A agarose was added to the lysate, and the mixture was incubated at 4°C for 4 hours. The agarose complexes containing antibodies, target proteins, and RNA were washed 3 times for 5 min at 4°C and repeated. Protein-bound RNA was extracted using RNAiso Plus and a Direct-zol RNA MicroPrep Kit. RIP–qPCR was performed according to the above RT–qPCR protocol.

Statistical analyses

Pearson's correlation coefficients (R) were calculated by using the scores of the two samples for MS. GraphPad Prism software (version 9.0.0) was used for the statistical analyses, and the values and error bars represent the mean ± SEM. Significant differences between the two groups were analysed using Student's *t* test. Statistical significance is indicated as follows: exact P value $P \geq 0.05$; $^{*}P < 0.05$; $^{**}P < 0.01$; $^{***}P < 0.001$; $^{****}P < 0.0001$).

Data availability

All data generated or analysed during this study are included in this published article, its supplementary information files and publicly available repositories. Mass spec data are included in supplementary information files (Table S7). The RNA-seq data were deposited in GEO (https://www.ncbi.nlm.nih.gov/geo/) under accession number GSE227575. The CLIP-seq data were deposited in GEO under accession number GSE227422 (Sun *et al.*, 2023a).

Acknowledgments

This work was supported by the National Natural Science Foundation of China (32171111); and the Beijing Natural Science Foundation (5222015). We thank Prof. Yuanchao Xue (Institute of Biophysics, Chinese Academy of Sciences, Beijing, China) for sharing *Srsf1*$^{Fl/Fl}$ mice, Prof. Shuyang Yu, Hua Zhang and Chao Wang (China Agricultural University, Beijing, China) for thoughtful discussions and suggestions, and all the members of Prof. Hua Zhang, Chao Wang, and Shuyang Yu laboratory for helpful discussions and comments. We thank Novogene for their assistance with the RNA-seq and CLIP-seq experiments.

References

Beck, A.R., Miller, I.J., Anderson, P., and Streuli, M. (1998). RNA-binding protein TIAR is essential for primordial germ cell development. Proc Natl Acad Sci U S A *95*, 2331-2336. 10.1073/pnas.95.5.2331.

Cafe, S.L., Skerrett-Byrne, D.A., De Oliveira, C.S., Nixon, B., Oatley, M.J., Oatley, J.M., and Lord, T. (2021). A regulatory role for CHD4 in maintenance of the spermatogonial stem cell pool. Stem cell reports *16*, 1555-1567. 10.1016/j.stemcr.2021.04.003.

Chen, Y., Zheng, Y., Gao, Y., Lin, Z., Yang, S., Wang, T., Wang, Q., Xie, N., Hua, R., Liu, M., et al. (2018). Single-cell RNA-seq uncovers dynamic processes and critical regulators in mouse spermatogenesis. Cell Res *28*, 879-896. 10.1038/s41422-018-0074-y.

Du, J.X., Luo, Y.H., Zhang, S.J., Wang, B., Chen, C., Zhu, G.Q., Zhu, P., Cai, C.Z., Wan, J.L., Cai, J.L., et al. (2021). Splicing factor SRSF1 promotes breast cancer progression via oncogenic splice switching of PTPMT1. J Exp Clin Cancer Res *40*, 171. 10.1186/s13046-021-01978-8.

Gagliardi, M., and Matarazzo, M.R. (2016). RIP: RNA Immunoprecipitation. Methods Mol Biol *1480*, 73-86. 10.1007/978-1-4939-6380-5_7.

Gallardo, T., Shirley, L., John, G.B., and Castrillon, D.H. (2007). Generation of a germ cell-specific mouse transgenic Cre line, Vasa-Cre. Genesis (New York, N.Y. : 2000) *45*, 413-417. 10.1002/dvg.20310.

Goertz, M.J., Wu, Z., Gallardo, T.D., Hamra, F.K., and Castrillon, D.H. (2011). Foxo1 is required in mouse spermatogonial stem cells for their maintenance and the initiation of spermatogenesis. J Clin Invest *121*, 3456-3466. 10.1172/jci57984.

Jiao, S.Y., Yang, Y.H., and Chen, S.R. (2021). Molecular genetics of infertility: loss-of-function mutations in humans and corresponding knockout/mutated mice. Hum Reprod Update *27*, 154-189. 10.1093/humupd/dmaa034.

Juul, A., Almstrup, K., Andersson, A.M., Jensen, T.K., Jorgensen, N., Main, K.M., Rajpert-De Meyts, E., Toppari, J., and Skakkebaek, N.E. (2014). Possible fetal determinants of male infertility. Nature reviews. Endocrinology *10*, 553-562. 10.1038/nrendo.2014.97.

Kanatsu-Shinohara, M., and Shinohara, T. (2013). Spermatogonial stem cell self-renewal and development. Annual review of cell and developmental biology *29*, 163-187. 10.1146/annurev-cellbio-101512-122353.

Katsuyama, T., Li, H., Comte, D., Tsokos, G.C., and Moulton, V.R. (2019). Splicing factor SRSF1 controls T cell hyperactivity and systemic autoimmunity. J Clin Invest *129*, 5411-5423. 10.1172/JCI127949.

Katsuyama, T., and Moulton, V.R. (2021). Splicing factor SRSF1 is indispensable for regulatory T cell homeostasis and function. Cell Rep *36*, 109339. 10.1016/j.celrep.2021.109339.

610 Kluin, P.M., and de Rooij, D.G. (1981). A comparison between the morphology and cell kinetics
611 of gonocytes and adult type undifferentiated spermatogonia in the mouse. International
612 journal of andrology *4*, 475-493. 10.1111/j.1365-2605.1981.tb00732.x.
613 La, H.M., and Hobbs, R.M. (2019a). Mechanisms regulating mammalian spermatogenesis and
614 fertility recovery following germ cell depletion. Cell Mol Life Sci *76*, 4071-4102.
615 10.1007/s00018-019-03201-6.
616 La, H.M., and Hobbs, R.M. (2019b). Mechanisms regulating mammalian spermatogenesis and
617 fertility recovery following germ cell depletion. Cell Mol Life Sci *76*, 4071-4102.
618 10.1007/s00018-019-03201-6.
619 Law, N.C., Oatley, M.J., and Oatley, J.M. (2019). Developmental kinetics and transcriptome
620 dynamics of stem cell specification in the spermatogenic lineage. Nat Commun *10*, 2787.
621 10.1038/s41467-019-10596-0.
622 Lee, J., and Shinohara, T. (2011). Epigenetic modifications and self-renewal regulation of
623 mouse germline stem cells. Cell Res *21*, 1164-1171. 10.1038/cr.2011.111.
624 Legrand, J.M.D., Chan, A.L., La, H.M., Rossello, F.J., Anko, M.L., Fuller-Pace, F.V., and Hobbs,
625 R.M. (2019). DDX5 plays essential transcriptional and post-transcriptional roles in the
626 maintenance and function of spermatogonia. Nat Commun *10*, 2278. 10.1038/s41467-019-
627 09972-7.
628 Lin, H., Cheng, K., Kubota, H., Lan, Y., Riedel, S.S., Kakiuchi, K., Sasaki, K., Bernt, K.M.,
629 Bartolomei, M.S., Luo, M., and Wang, P.J. (2022). Histone methyltransferase DOT1L is
630 essential for self-renewal of germline stem cells. Genes Dev *36*, 752-763.
631 10.1101/gad.349550.122.
632 Liu, J., You, M., Yao, Y., Ji, C., Wang, Z., Wang, F., Wang, D., Qi, Z., Yu, G., Sun, Z., et al. (2021).
633 SRSF1 plays a critical role in invariant natural killer T cell development and function. Cell Mol
634 Immunol *18*, 2502-2515. 10.1038/s41423-021-00766-w.
635 Liu, W., Lu, X., Zhao, Z.H., Su, R., Li, Q.L., Xue, Y., Gao, Z., Sun, S.S., Lei, W.L., Li, L., et al. (2022).
636 SRSF10 is essential for progenitor spermatogonia expansion by regulating alternative splicing.
637 eLife *11*. 10.7554/eLife.78211.
638 Liu, W., Wang, F., Xu, Q., Shi, J., Zhang, X., Lu, X., Zhao, Z.A., Gao, Z., Ma, H., Duan, E., et al.
639 (2017). BCAS2 is involved in alternative mRNA splicing in spermatogonia and the transition to
640 meiosis. Nat Commun *8*, 14182. 10.1038/ncomms14182.
641 Lv, Y., Zhang, W., Zhao, J., Sun, B., Qi, Y., Ji, H., Chen, C., Zhang, J., Sheng, J., Wang, T., et al.
642 (2021). SRSF1 inhibits autophagy through regulating Bcl-x splicing and interacting with PIK3C3
643 in lung cancer. Signal Transduct Target Ther *6*, 108. 10.1038/s41392-021-00495-6.
644 Mazin, P.V., Khaitovich, P., Cardoso-Moreira, M., and Kaessmann, H. (2021). Alternative
645 splicing during mammalian organ development. Nat Genet *53*, 925-934. 10.1038/s41588-021-
646 00851-w.
647 McLean, D.J., Friel, P.J., Johnston, D.S., and Griswold, M.D. (2003). Characterization of
648 spermatogonial stem cell maturation and differentiation in neonatal mice. Biol Reprod *69*,
649 2085-2091. 10.1095/biolreprod.103.017020.
650 Merkin, J., Russell, C., Chen, P., and Burge, C.B. (2012). Evolutionary dynamics of gene and
651 isoform regulation in Mammalian tissues. Science *338*, 1593-1599. 10.1126/science.1228186.
652 Oatley, J.M., and Brinster, R.L. (2012). The germline stem cell niche unit in mammalian testes.
653 Physiological reviews *92*, 577-595. 10.1152/physrev.00025.2011.
654 Qi, Z., Wang, F., Yu, G., Wang, D., Yao, Y., You, M., Liu, J., Liu, J., Sun, Z., Ji, C., et al. (2021).
655 SRSF1 serves as a critical posttranscriptional regulator at the late stage of thymocyte
656 development. Sci Adv *7*. 10.1126/sciadv.abf0753.
657 Qin, J., Huang, T., Wang, J., Xu, L., Dang, Q., Xu, X., Liu, H., Liu, Z., Shao, C., and Zhang, X. (2022).
658 RAD51 is essential for spermatogenesis and male fertility in mice. Cell death discovery *8*, 118.
659 10.1038/s41420-022-00921-w.

660 Qin, J., Huang, T., Wang, Z., Zhang, X., Wang, J., Dang, Q., Cui, D., Wang, X., Zhai, Y., Zhao, L.,
661 et al. (2023). Bud31-mediated alternative splicing is required for spermatogonial stem cell self-
662 renewal and differentiation. Cell Death Differ *30*, 184-194. 10.1038/s41418-022-01057-1.
663 Song, H., Wang, L., Chen, D., and Li, F. (2020). The Function of Pre-mRNA Alternative Splicing
664 in Mammal Spermatogenesis. Int J Biol Sci *16*, 38-48. 10.7150/ijbs.34422.
665 Song, H.W., and Wilkinson, M.F. (2014). Transcriptional control of spermatogonial
666 maintenance and differentiation. Seminars in cell & developmental biology *30*, 14-26.
667 10.1016/j.semcdb.2014.02.005.
668 Sun, L., Chen, J., Ye, R., Lv, Z., Chen, X., Xie, X., Li, Y., Wang, C., Lv, P., Yan, L., et al. (2023a).
669 SRSF1 is crucial for male meiosis through alternative splicing during homologous pairing and
670 synapsis in mice. Science bulletin *68*, 1100-1104. 10.1016/j.scib.2023.04.030.
671 Sun, L., Lv, Z., Chen, X., Wang, C., Lv, P., Yan, L., Tian, S., Xie, X., Yao, X., Liu, J., et al. (2023b).
672 SRSF1 regulates primordial follicle formation and number determination during meiotic
673 prophase I. BMC Biol *21*, 49. 10.1186/s12915-023-01549-7.
674 Tan, K., and Wilkinson, M.F. (2020). A single-cell view of spermatogonial stem cells. Current
675 opinion in cell biology *67*, 71-78. 10.1016/j.ceb.2020.07.005.
676 Venables, J.P. (2002). Alternative splicing in the testes. Current opinion in genetics &
677 development *12*, 615-619. 10.1016/s0959-437x(02)00347-7.
678 Wang, E.T., Sandberg, R., Luo, S., Khrebtukova, I., Zhang, L., Mayr, C., Kingsmore, S.F., Schroth,
679 G.P., and Burge, C.B. (2008). Alternative isoform regulation in human tissue transcriptomes.
680 Nature *456*, 470-476. 10.1038/nature07509.
681 Wang, X., Liu, X., Qu, M., and Li, H. (2023). Sertoli cell-only syndrome: advances, challenges,
682 and perspectives in genetics and mechanisms. Cell Mol Life Sci *80*, 67. 10.1007/s00018-023-
683 04723-w.
684 Wang, Y.H., Yan, M., Zhang, X., Liu, X.Y., Ding, Y.F., Lai, C.P., Tong, M.H., and Li, J.S. (2021).
685 Rescue of male infertility through correcting a genetic mutation causing meiotic arrest in
686 spermatogonial stem cells. Asian J Androl *23*, 590-599. 10.4103/aja.aja_97_20.
687 Wang, Z., Xu, X., Li, J.L., Palmer, C., Maric, D., and Dean, J. (2019). Sertoli cell-only phenotype
688 and scRNA-seq define PRAMEF12 as a factor essential for spermatogenesis in mice. Nat
689 Commun *10*, 5196. 10.1038/s41467-019-13193-3.
690 Xu, K., Yang, Y., Feng, G.H., Sun, B.F., Chen, J.Q., Li, Y.F., Chen, Y.S., Zhang, X.X., Wang, C.X.,
691 Jiang, L.Y., et al. (2017). Mettl3-mediated m(6)A regulates spermatogonial differentiation and
692 meiosis initiation. Cell Res *27*, 1100-1114. 10.1038/cr.2017.100.
693 Xu, X., Yang, D., Ding, J.H., Wang, W., Chu, P.H., Dalton, N.D., Wang, H.Y., Bermingham, J.R.,
694 Jr., Ye, Z., Liu, F., et al. (2005). ASF/SF2-regulated CaMKIIdelta alternative splicing temporally
695 reprograms excitation-contraction coupling in cardiac muscle. Cell *120*, 59-72.
696 10.1016/j.cell.2004.11.036.
697 Yamaji, M., Jishage, M., Meyer, C., Suryawanshi, H., Der, E., Yamaji, M., Garzia, A., Morozov,
698 P., Manickavel, S., McFarland, H.L., et al. (2017). DND1 maintains germline stem cells via
699 recruitment of the CCR4-NOT complex to target mRNAs. Nature *543*, 568-572.
700 10.1038/nature21690.
701 Yan, Y., Zhang, D., Zhou, P., Li, B., and Huang, S.Y. (2017). HDOCK: a web server for protein-
702 protein and protein-DNA/RNA docking based on a hybrid strategy. Nucleic Acids Res *45*,
703 W365-w373. 10.1093/nar/gkx407.
704 Zhou, S., Dong, J., Xiong, M., Gan, S., Wen, Y., Zhang, J., Wang, X., Yuan, S., and Gui, Y. (2022).
705 UHRF1 interacts with snRNAs and regulates alternative splicing in mouse spermatogonial stem
706 cells. Stem cell reports *17*, 1859-1873. 10.1016/j.stemcr.2022.06.010.

707